Research paper

Spectral distortions in zinc-based metal-enhanced fluorescence underpinned by fast and slow electronic transitions

Rachael Knoblauch[a], Hilla Ben Hamo[b], Robert Marks[b], Chris D. Geddes[a,*]

[a] *Institute of Fluorescence and Department of Chemistry and Biochemistry, University of Maryland Baltimore County, 701 East Pratt Street, Baltimore, MD 21202, USA*
[b] *Department of Biotechnology Engineering, Faculty of Engineering Sciences, Ben-Gurion University of the Negev, Be'er Sheva, Israel*

HIGHLIGHTS

- Zinc nanoparticulate films yield spectral distortion in Metal-Enhanced Fluorescence.
- Both red edge and blue edge distortions are observed from Rose Bengal emission.
- Favored enhancement of slow (red) and fast (blue) transitions causes distortion.

ARTICLE INFO

ABSTRACT

Metal-enhanced fluorescence (MEF) is a promising technology with impact in diagnostics, electronics, and sensing. Despite investigation into MEF fundamentals, some properties remain unresearched, notably spectral distortion. To date, publications have described its underpinnings, yet comprehensive analysis is needed, as presented recently for silver films. Herein we expand this description using zinc substrates (ZnNPs). Significant red-edge and blue-edge distortions are reported using Rose Bengal. Radiative decay rate modification is identified as key in amplifying fast/slow electronic transitions by the enhanced emission mechanism. Furthermore, we identify distortion in published studies, bolstering our thinking that spectral distortion is an intrinsic property of MEF.

1. Introduction

In recent years, metal-enhanced fluorescence (MEF) has become a ubiquitous technology in fields spanning diagnostics to electronics [1–3], and which is underpinned by both an enhanced absorption and emission mechanism [4]. For enhanced absorption, plasmon excitation creates near-fields which subsequently excite larger volumes of fluorophore solution than is possible in free-space (FS) conditions [5,6]. By the enhanced emission mechanism, fluorophores couple to and induce surface plasmon oscillations, yielding modified fluorophore-nanoparticle decay rates with increased quantum yields for the coupled system [7–9]. Although early MEF research focused on understanding fundamentals of fluorophore-plasmon coupling, recent studies have focused largely on tuning the fluorophore-nanoparticle system for their applications. Subsequently, the spectral distortions observed in MEF systems have only lightly been addressed *hitherto*. Modified decay rate, metal nanoparticle scattering, and spectral overlap effects have been implicated [10–13], yet these studies in isolation do not present an overall description of MEF spectral modification. In a recent report, we provided a wholistic analysis of spectral distortion in MEF using silver nanoparticle geometries (Knoblauch, R.; Hamo, H. B.; Marks, R.; Geddes, C. D., Spectral Distortions in Metal-Enhanced Fluorescence: Experimental Evidence for Ultra-Fast and Slow Transitions. *J. Phys. Chem. C.,* accepted for publication, Feb. 2020.); however, spectral distortion is also evident in MEF from other metals [14–17]. In fact, a study by our lab in 2015 reported significant red-edge distortion in the enhanced spectra of Basic Fuchsin on zinc nanoparticle substrates [14]. To further build upon and understand distortion from zinc, we have subsequently investigated the spectral characteristics of Rose Bengal on zinc films.

2. Results & Discussion

Solutions of Rose Bengal (10 µM, deionized water) were placed on

---

Abbreviations: MEF, metal-enhanced fluorescence; CF, coupled fluorescence; EF, enhancement factor; ZnNPs, zinc nanoparticle substrate (For additional acronyms and abbreviations, see the supplemental material Appendix A.)

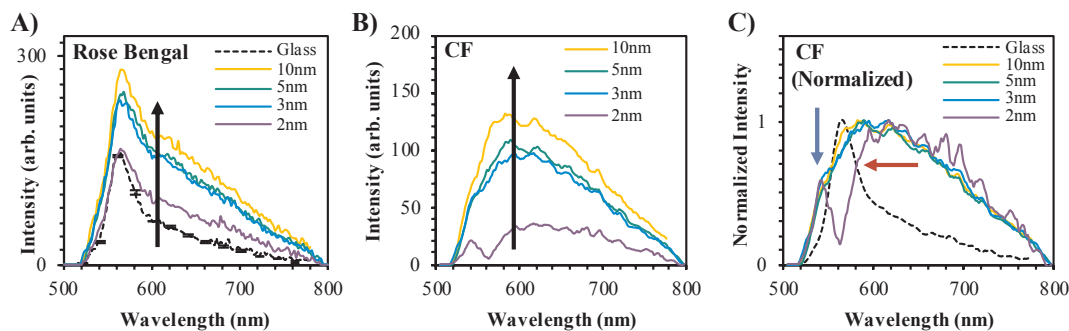* Corresponding author.
  E-mail address: geddes@umbc.edu (C.D. Geddes).

Fig. 1. Metal-enhanced fluorescence (MEF) from Rose Bengal (λ_{ex} = 405 nm) detected on glass or zinc nanoparticle-coated substrates (ZnNPs) of varying thicknesses. (*A*) MEF response from fluorophore solutions on varying ZnNPs. (*B*) Coupled fluorescence (CF) spectra calculated for each film. (*C*) Normalized CF spectra for each film compared to raw spectrum detected on glass. Blue-edge (blue arrow) and red-edge (red arrow) distortion are identified. (For interpretation of the references to colour in this figure legend, the reader is referred to the web version of this article.)

Table 1
Enhancement Factors from Metal-Enhanced Fluorescence of Rose Bengal on Zinc Nanoparticulate Films Reported for Different Emission Wavelengths.

Film Thickness	$EF_{542\ nm}$	$EF_{566\ nm}$	$EF_{670\ nm}$
2 nm	1.81	1.05	2.13
3 nm	2.81	1.43	3.23
5 nm	2.77	1.52	3.38
10 nm	3.11	1.74	3.85

zinc nanoparticle films (ZnNPs) of 2–10 nm thicknesses and the fluorescence detected. As predicted, there is significant increase in fluorescence for ZnNP systems as compared to free-space fluorescence (Fig. 1a), i.e. metal-enhanced fluorescence. This is observed for all films, with a definitive increase in MEF as a function of thickness. Wavelength-dependence is also observed (Fig. S2a–d), indicating spectral modification for this MEF system. Enhancement factors (EF) at select wavelengths are reported in Table 1.

The "coupled fluorescence" (CF) spectrum for each system was subsequently isolated by subtracting free-space intensities from each MEF spectrum (Fig. 1b, S2). This approximation is permissible as MEF is through-space, with ≪1% of solution actually within the enhancement region volume [18–20]. Although red-edge distortion is evident in the MEF spectra, the CF spectra reveal significant variation on *both* the red- and remarkably blue-edges, particularly for 2-nm films (Fig. 1c).

There are several potential sources of spectral modification discussed in the literature which could explain what is observed here. In 2010, Le Ru et al. speculated that overlap of the metal localized surface plasmon resonance (LSPR) band and fluorophore emission wavelengths could cause distortion in MEF, although these suggestions have not been experimentally verified until now [11]. The authors suggested that strong LSPR wavelengths would couple efficiently to fluorophore emission, modifying the fluorophore decay rate. Association to much shorter lifetimes of excited plasmons increases the decay rates of slower emissive pathways, thereby enhancing weaker signals preferentially. This process was described as "slow dynamics" MEF (SD MEF) by Le Ru et al. and is depicted schematically in Fig. 2. To study this, both the absorption and $\lambda_{ex} = \lambda_{em}$ spectra of the ZnNPs were recorded (Fig. S3). Although Le Ru discusses specifically absorption alone, it has been shown in the literature that MEF wavelength dependence correlates more closely to the scattering portion of the extinction spectrum [12,21].

The absorption spectra exhibit LSPR primarily in the ultra-violet (UV) range and reveal no structure in the visible region to indicate preferential coupling of Rose Bengal emission. This is predicted, as zinc nanoparticles are of interested due to favorable UV LSPR properties [22,23]. Conversely, $\lambda_{ex} = \lambda_{em}$ is in the visible region, which could provide the basis to support Le Ru's prediction, yet MEF wavelength-
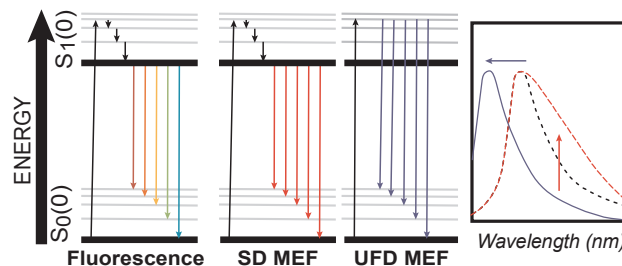

Fig. 2. Modified Jablonski diagram showing the transitions possible for coupling to metal nanoparticles in metal-enhanced fluorescence (MEF). Diagrams depict slow dynamics (SD) MEF and ultra-fast dynamics (UFD) MEF, as well as classical free-space fluorescence.

dependence does not correlate to $\lambda_{ex} = \lambda_{em}$ as enhancement of $\lambda_{max,FS}$ would be expected in all CF spectra. While this is detectable for 3–10 nm ZnNPs, it is not the case for 2-nm films (Fig. 1, S2). This observation is explained if one considers that Rose Bengal has a low quantum yield, indicating a significant contribution of non-radiative decay to the overall decay rate of an excited fluorophore. By introducing an alternate radiative decay pathway (MEF) that is hallmarked by the short lifetimes of metal plasmons, radiative decay becomes more competitive. At $\lambda_{max,FS}$ this effect should be the least pronounced in the CF spectrum due to the relatively high probability of radiative emission. In 2-nm films, weaker transitions are amplified, verifying decay rate modification as a possible mechanism for red-edge distortion. In the larger particle films $\lambda_{max,FS}$ becomes dominant in the CF spectra, which will be addressed later.

In order to further elucidate the relative electronic transitions amplified in the CF spectra, multi-Gaussian deconvolution analysis was performed for each condition as shown in Fig. 3. It is interesting to note that the 2-nm CF spectrum displays a strong *hypsochromic* signal (~546 nm), that is not present in the glass spectra (control substrate). Blue-edge distortion has been observed far less commonly than red-edge distortion, although it has been theoretically predicted (Knoblauch et al,. *J. Phys. Chem. C.,* accepted for publication, Feb. 2020.) [10,11]. In a process termed "ultra-fast" dynamics MEF (UFD MEF), Le Ru proposes that high-energy emission is observed by decay rate modification [11].

Typically, excitation occurs to non-zero vibronic states, $S_1(\omega)$, decaying non-radiatively to $S_1(0)$ before emitting (Fig. 2). In the case of UFD MEF, Le Ru proposed that excited fluorophores coupled to plasmons may radiate so quickly that rapid emission becomes competitive to internal conversion ($S_1(\omega) \rightarrow S_1(0)$). Emission then occurs from much higher energy states than free-space, yielding blue-edge distortion. This would occur only for those fluorophores whose quanta are coupled to plasmons, and therefore should be observed when metal
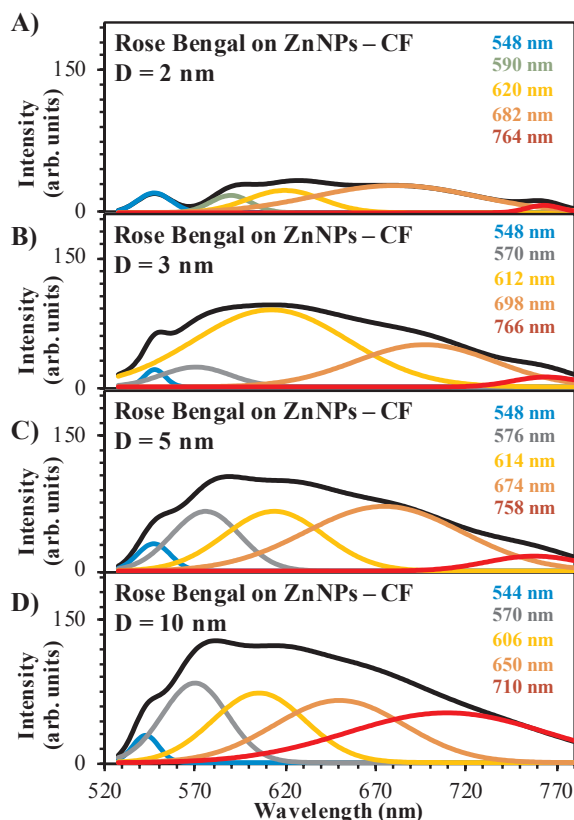
Fig. 3. Multi-Gaussian deconvolution analysis of the coupled fluorescence (CF) spectra for Rose Bengal (λ_{ex} = 405 nm) excited on zinc nanoparticle-coated substrates (ZnNPs) of varying nanoparticle film thicknesses including (*A*) 2, (*B*) 3, (*C*) 5, and (*D*) 10 nm. Cumulative fits are shown in black; component peaks are shown in color. Corresponding peak wavelengths are indicated by the colored inset labels. For fit information, see supplemental figure S4. (For interpretation of the references to colour in this figure legend, the reader is referred to the web version of this article.)

scattering of blue-edge wavelengths is favorable. Interestingly, the $\lambda_{ex} = \lambda_{em}$ profile of ZnNPs reveals strongest scattering at the blue-edge of Rose Bengal emission (Fig. S2b). The 2-nm CF spectrum thusly reveals *both* bathochromic and hypsochromic spectral distortions, which together implicate enhancement *and* decay rate modification from the coupled system.

When examining the CF spectra from 3 to 10 nm films, the hypsochromic distortions are minimal (Figs. 1,3). In fact, as with many reports of MEF, blue-edge distortion may not be observable at all when comparing the MEF spectrum against the control sample (Fig. S2). This could imply that efficiency of *coupling* between excited fluorophores and nanoparticle plasmons is not impacted by variation of the zinc particle size within these conditions. When examining trends in integrated intensity for $\lambda_{max,FS}$ and the red edge, this consistency is not observed. The integrated intensity of $\lambda_{max,FS}$ instead increases sharply with film thickness, while red-edge intensities also increase (Fig. 3, S5b-c). This may be explained if one also considers the enhanced *absorption* mechanism as a source of spectral modification, where direct coupling of the fluorophore-nanoparticle system is not required. Fluorophores enhanced exclusively by this mechanism should, theoretically, exhibit characteristics akin to free-space emission since enhancement occurs by increasing the probability of excitation events [5,24]. In realistic systems both enhanced absorption and enhanced emission mechanisms contribute to MEF. In order to probe the enhanced absorption mechanism, the free-space spectrum also underwent multi-Gaussian deconvolution analysis for comparison to CF spectra (Fig. 4a, S4). Component peak percent area contributions were also calculated (Fig. 4b,
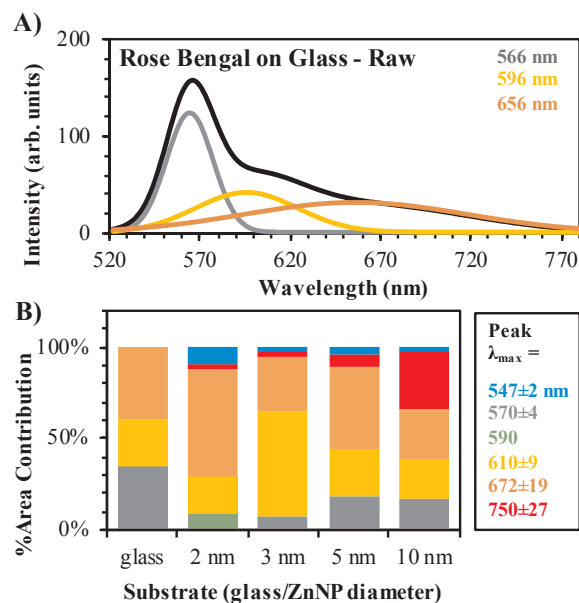

Fig. 4. Analysis of the red-shifted fluorescence contribution for Rose Bengal excited on glass versus zinc nanoparticle-coated substrates ("ZnNPs," λ_{ex} = 405 nm) of varying nanoparticle film thicknesses. (*A*) Multi-Gaussian deconvolution analysis of the raw fluorescence from Rose Bengal excited on glass. Cumulative fits are shown in black; component peaks are shown in color. Corresponding peak wavelengths are indicated by the colored inset labels. For fit information, see supplemental figure S3. (*B*) Percent integrated area contribution of each peak component identified in the deconvolution spectra of glass versus ZnNP systems (Fig. 3). (For interpretation of the references to colour in this figure legend, the reader is referred to the web version of this article.)

Table S1). It can be seen that red-edge wavelengths contribute to free-space emission; however, the $\lambda_{max,FS}$ component contributes overall 34.3% of the total integrated area of the fit equation. For 3–10 nm film thicknesses, the $\lambda_{max,FS}$ component peak is still present, although the percent contribution is less than the free-space emission profile with more dominant red-edge wavelengths. Blue-edge distortion is also detected for 3–10 nm films, albeit at lower contributions as compared to red-edge or $\lambda_{max,FS}$ peaks. These results are expected if MEF is due to a combined enhanced emission and absorption mechanism [24]. While blue-edge distortion is due to enhanced emission and coupling, $\lambda_{max,FS}$ and red-edge wavelengths can be enhanced via either mechanism. Subsequently, contributions from these peaks increase with film thickness as excitation volume regions from nanoparticle scattering expand due to the enhanced absorption mechanism, (Fig. S3) [5,22]. The probability of coupling, conversely, is a near-field phenomenon that may not vary greatly with thickness, as observed for the blue-edge contributions.

As such, free-space spectral characteristics are enhanced for thicker films, masking weaker distortion from coupled systems, and the CF spectra begin to more closely resemble free-space emission. It is also of note that CF spectral analysis was performed from data reported by our lab in 2015, for Basic Fuchsin detected on ZnNPs (Fig. S6) [14]. Red-edge distortion is observed, with red-shifted component peaks (the blue-edge peak is an exception, blue-shifting in the CF spectrum). Interestingly, percent contribution increases most significantly for $\lambda_{max,FS}$ compared to the other components (Fig. S6d). This is of particular note, as Basic Fuchsin has a higher quantum yield than Rose Bengal and therefore should be less impacted by coupling and decay rate modification, leading to more free-space spectral characteristics [25]. In contrast, the 2-nm films of this study have no detectable $\lambda_{max,FS}$ peak, possibly indicating a dominant enhanced emission mechanism.

3. Conclusion

Herein we have reported the detection of significant bathochromic and hypsochromic distortion in the MEF spectrum of Rose Bengal on ZnNPs. MEF spectral distortion is further analyzed by isolating the coupled fluorescence spectra, representing *only* the fluorescence from enhancement mechanisms. Contribution of the enhanced absorption and emission mechanisms in determining MEF spectral profile is discussed, pinpointing decay rate modification for both fast and slow transitions as a cause of significant distortion effects. Although this has been reported for silver substrates and platinum (Fig. S7) [15] previously, that this distortion is observed also on zinc nanoparticle substrates begins to implicate spectral distortion as potential window to further understanding the fluorophore-metal interplay and the complex mechanism of MEF.

4. Experimental methods

Rose Bengal and 99.995% pure zinc were purchased from Sigma-Aldrich and the Kurt J. Lesker Company respectively. Zinc nanoparticles were deposited on glass slides by thermal vapor deposition according to a previously published procedure (Knoblauch et al,. *J. Phys. Chem. C.,* accepted for publication, Feb. 2019.) [14]. A Cary 60 Bio UV–Vis spectrophotometer was used to record the absorbance spectra with slide surfaces oriented perpendicular to the beam. The synchronous scattering spectra, or spectra recorded when emission and excitation wavelengths are equal ($\lambda_{ex} = \lambda_{em}$), were obtained by mounting slides on absorptive neutral density filters within the plate reader of a Cary Eclipse Varian spectrophotometer. Fluorescence was recorded on a HR 2000 spectrograph from Ocean Optics. Samples were excited perpendicular to the surface using a 405-nm laser; emission was collected through a 510-nm long pass filter at a 45° angle (Fig. S1). Intensities were extracted from images by a converted grid method whereby pixel counts were ascribed to both axes and data intensities, and true values were calculated from the pixel to intensity ratio (described in a previous publication: Knoblauch et al,. *J. Phys. Chem. C.,* accepted for publication, Feb. 2019.). The "coupled fluorescence" (CF) spectrum for each system was isolated by subtracting free-space intensities from each MEF spectrum. This approximation is permissible as MEF is through-space, with ≪1% of solution actually within the enhancement region volume [18–20]. The CF spectra were then subject to multi-Gaussian deconvolution analysis, with fits optimized against R^2 and residual values. Percent area contribution was calculated from the integrated intensities of each component peak and are reported in conjunction with the corresponding maximum intensity wavelength (λ_{max}).

Author contributions

All information reported was written by Rachael Knoblauch and edited by Dr. Chris D. Geddes. All experiments were conducted by Hilla Ben Hamo under the direction of Dr. Chris D. Geddes, while under the mentorship of Robert Marks. Data extraction, analysis and calculations were completed by Rachael Knoblauch.

CRediT authorship contribution statement

Rachael Knoblauch: Formal analysis, Data curation, Writing - original draft, Writing - review & editing, Visualization, Funding acquisition. **Hilla Ben Hamo:** Validation, Investigation, Data curation. **Robert Marks:** Supervision, Project administration. **Chris D. Geddes:** Conceptualization, Methodology, Validation, Resources, Writing - review & editing, Supervision, Project administration, Funding acquisition.

Declaration of Competing Interest

The authors declare that they have no known competing financial interests or personal relationships that could have appeared to influence the work reported in this paper.

Appendix A. Supplementary material

Supplementary data to this article can be found online at https://doi.org/10.1016/j.cplett.2020.137212.

References

[1] Y. Jeong, Y.-M. Kook, K. Lee, W.-G. Koh, Metal enhanced fluorescence (MEF) for biosensors: General approaches and a review of recent developments, Biosens. Bioelectron. 111 (2018) 102–116.

[2] P. Strobbia, E. Languirand, B.M. Cullum, Recent advances in plasmonic nanostructures for sensing: a review, Opt. Eng. 54 (10) (2015) 100902.

[3] L. Sai, W. Ziwei, Z. Yijun, H. Yunyun, Y. Rongrong, X. Weidong, Z. Yongqiang, Easy synthesis of silver nanoparticles-orange emissive carbon dots hybrids exhibiting enhanced fluorescence for white light emitting diodes, J. Alloy. Compd. 700 (2017) 75–82.

[4] K. Aslan, C.D. Geddes, Metal-enhanced fluorescence: progress towards a unified plasmon-fluorophore description, in: C.D. Geddes (Ed.), Metal-Enhanced Fluorescence, John Wiley & Sons Inc, Hoboken, New Jersey, 2010, pp. 1–23.

[5] A.I. Dragan, C.D. Geddes, Excitation volumetric effects (EVE) in metal-enhanced fluorescence, PCCP 13 (9) (2011) 3831–3838.

[6] M. Weisenberg, Y. Zhang, C.D. Geddes, Metal-enhanced chemiluminescence from chromium, copper, nickel, and zinc nanodeposits: evidence for a second enhancement mechanism in metal-enhanced fluorescence, Appl. Phys. Lett. 97 (13) (2010) 133103.

[7] A.I. Dragan, C.D. Geddes, Metal-enhanced fluorescence: The role of quantum yield, Q0, in enhanced fluorescence, Appl. Phys. Lett. 100 (9) (2012) 093115.

[8] J.O. Karolin, C.D. Geddes, Reduced lifetimes are directly correlated with excitation irradiance in metal-enhanced fluorescence (MEF), J. Fluoresc. 22 (6) (2012) 1659–1662.

[9] L.-Y. Wei, K.-S. Huang, H.-H. Ling, Y.-P. Wu, K.-T. Tan, Y.Y. Lee, I.C. Chen, Kinetic mechanism of metal enhanced fluorescence by gold nanoparticle with Avidin-Biotin as spacer and by gold-silver core-shell nanoparticle using fluorescence lifetime image microscopy, J. Phys. Chem. C 122 (49) (2018) 28431–28438.

[10] E.C. Le Ru, P.G. Etchegoin, J. Grand, N. Félidj, J. Aubard, G. Lévi, Mechanisms of spectral profile modification in surface-enhanced fluorescence, J. Phys. Chem. C 111 (2007) 16076–16079.

[11] E.C. Le Ru, J. Grand, N. Félidj, J. Aubard, G. Lévi, A. Hohenau, J.R. Krenn, E. Blackie, P.G. Etchegion, Spectral profile modifications in metal-enhanced fluorescence, John Wiley & Sons, Inc., Hoboken, New Jersey, 2010, pp. 25–66.

[12] A.I. Dragan, B. Mali, C.D. Geddes, Wavelength-dependent metal-enhanced fluorescence using synchronous spectral analysis, Chem. Phys. Lett. 556 (2013) 168–172.

[13] R. Knoblauch, E. Ra, C.D. Geddes, Heavy carbon nanodots 2: plasmon amplification in Quanta Plate™ wells and the correlation with the synchronous scattering spectrum, Phys. Chem. Chem. Phys. 21 (3) (2019) 1254–1259.

[14] H. Ben Hamo, A. Kushmaro, R. Marks, J. Karolin, B. Mali, C.D. Geddes, Metal-enhanced fluorescence from zinc substrates can lead to spectral distortion and a wavelength dependence, Appl. Phys. Lett. 106 (8) (2015).

[15] N. Akbay, F. Mahdavi, J.R. Lakowicz, K. Ray, Metal-enhanced intrinsic fluorescence of nucleic acids using platinum nanostructured substrates, Chem. Phys. Lett. 548 (2012) 45–50.

[16] C.D. Geddes, Spectral shifts in metal-enhanced fluorescence, Appl. Phys. Lett. 105 (6) (2014).

[17] K. Sugawa, T. Tamura, H. Tahara, D. Yamaguchi, T. Akiyama, J. Otsuki, Y. Kusaka, N. Fukuda, H. Ushijima, Metal-enhanced fluorescence platforms based on plasmonic ordered copper arrays: wavelength dependence of quenching and enhancement effects, ACS Nano 7 (11) (2013) 9997–10010.

[18] R. Knoblauch, C.D. Geddes, Silvered conical-bottom 96-well plates: enhanced low volume detection and the metal-enhanced fluorescence volume/ratio effect, Nanoscale 11 (10) (2019) 4337.

[19] H. Mishra, B.L. Mali, J. Karolin, A.I. Dragan, C.D. Geddes, Experimental and theoretical study of the distance dependence of metal-enhanced fluorescence,

phosphorescence and delayed fluorescence in a single system, Phys. Chem. Chem. Phys. 15 (2013) 19538–19544.

[20] A.I. Dragan, E.S. Bishop, J.R. Casas-Finet, R.J. Strouse, J. McGivney, M.A. Schenerman, C.D. Geddes, Distance dependence of metal-enhanced fluorescence, Plasmonics 7 (2012) 739–744.

[21] C.D. Geddes, Wavelength dependence of metal-enhanced fluorescence, J. Phys. Chem. C 113 (28) (2009) 12095–12100.

[22] K. Aslan, M.J.R. Previte, Z. Yongxia, C.D. Geddes, Metal-enhanced fluorescence from nanoparticulate zinc films, J. Phys. Chem. C 112 (47) (2008) 18368–18375.

[23] K. Aslan, C.D. Geddes, Surface plasmon coupled fluorescence in the ultraviolet and visible spectral regions using zinc thin films, Anal. Chem. 80 (19) (2008) 7304–7312.

[24] C.D. Geddes, Metal-enhanced Fluorescence, Wiley, Hoboken, N.J., 2010, p. c2010.

[25] B. Pathrose, V.P. Nampoori, P. Radhakrishnan, A. Mujeeb, Measurement of absolute fluorescence quantum yield of basic Fuchsin solution using a dual-beam thermal lens technique, J. Fluoresc. 24 (3) (2014) 895–898.